Model Experiments on Characteristics of Motions of Continuous Pontoon Type and Separate Support Type Elastic Floating Bodies in Waves

by

Haruo YONEYAMA [1], Satoru SHIRAISHI [2] and Go ISHIMI [3]

ABSTRACT

Several floating bridges, which have been recently put to practical use in the United States and Norway, are mainly classified into two types: a continuous pontoon type and a separate support type. It has been well known that long and large beam-like flexible floating structures such as these floating bridges show the characteristics of elastic deformations in waves. In this paper, hydraulic model experiments, which have been carried out to investigate the characteristics of motions of these two types of floating structure, are broadly reported.

KEY WORDS: Floating Bridge
Elastic Deformation
Elastic Floating Body
Rigid Floating body

1. INTRODUCTION

In recent years, various types of floating structure have been planned and constructed for the purpose of effective utilization in coastal areas. Floating structures can be generally considered as rigid floating bodies in estimating their motions in waves because of enough large rigidity of them. On the other hand, long flexible floating structures such as floating bridges have been developed and put to practical use mainly in the United States and Norway (Lwin, 1994; Landet, 1994). Besides, construction of the first floating bridge in Japan has started in Osaka (Maruyama et al., 1998a, 1998b). To evaluate the motions of these types of floating structure, it is improper to regard them as rigid floating bodies because of elastic properties of them. Namely, for dealing with long and large beam-like flexible floating structures such as floating bridges, it becomes necessary to examine the characteristics of their responses due to waves by taking account of elastic deformations of them.

The floating bridges are mainly classified into two types: a continuous pontoon type and a separate support type. The former is the type that consists of several floating box-type pontoons continuously arranged in one row on water surface. Meanwhile, the latter is the type that consists of several floating foundation pontoons arranged at intervals on water surface and a superstructure used as a road surface.

Photograph 1 shows a continuous pontoon type floating bridge called "Evergreen Point Bridge" which was constructed on Lake Washington in Seattle in the United States in 1963. This is one of three Lake Washington Floating Bridges. Since the bridge is composed of 33 prestressed concrete box-type pontoons rigidly connected

1)Senior Research Engineer, Structural Engineering Division, Port and Harbour Research Institute, Ministry of Transport, Nagase 3-1-1, Yokosuka 239-0826, Japan
2)Chief, Offshore Structures Laboratory, Structural Engineering Division, Port and Harbour Research Institute, Ministry of Transport
3)Former Member, Offshore Structures Laboratory, Structural Engineering Division, Port and Harbour Research Institute, Ministry of Transport (The Fifth District Port Construction Bureau, Ministry of Transport)

together, it is a continuous floating structure as a whole. The length of the bridge is 2,310 m, and it has four traffic lanes. Each pontoon is moored to the bottom of the lake by means of stretched anchor cables. This bridge is characterized by a draw span that is provided in the middle of the bridge for a ship navigating the lake.

Photograph 2 shows a separate support type floating bridge named "Bergsϕysund Bridge" which was constructed across a fjord in Norway in 1992. This is one of two floating bridges in Norway. The place where the bridge is located has a water depth of about 300m, and a sea state around the bridge is relatively calm. These characteristics are attributed to geographical features of fjords frequently seen in the west coast of Norway. In the place like this, a floating bridge is more economical than any other types of bridge. The superstructure of the bridge is supported by seven high strength lightweight concrete pontoons floating on sea surface. The bridge is also supported by flexible rods and multi-layer rubber bearings at both ends.

Long and large flexible floating structures could be used not only as floating bridges but also as floating port terminals or other applications in the future. To establish design methods for these floating structures, the effects of long and large flexible floating structures on elastic responses of them in waves need to be clarified. This paper reports the results of hydraulic model experiments on the continuous pontoon type and the separate support type elastic floating bodies (Shiraishi et al., 1996, 1997a, 1997b; Ishimi et al., 1999; Shiraishi et al., 1999).

2. CONTINUOUS PONTOON TYPE ELASTIC FLOATING BODY

(1) Hydraulic Model Experiments

a) Models of floating body

A continuous pontoon type elastic floating body in hydraulic model experiments is made of a polyurethane board to reproduce flexible properties of a floating bridge. The purpose of the experiments is to measure the hydraulic characteristics of elastic floating bodies, especially, their deformations and motions.

The view of a model employed here is illustrated in **Fig. 1**. This model is Model-B. The model consists of one thin rectangular floating board and two mooring poles. The floating board has two holes through which the mooring poles are installed to moor the board. The mooring poles are fixed at the bottom of an experimental basin. The board can freely go up and down along the mooring poles subjected to waves.

Table 1 shows six types of floating board. In the table, length, width, thickness, density and Young's modulus of each board are listed. The board length and thickness are 2.0m and 0.02m, respectively. The density and the widths of Model-A, B and C are 98.0 kg/m^3 and 0.1, 0.2 and 0.5m, respectively. The density and the widths of Model-D, E and F are 200.0 kg/m^3 and 0.1, 0.2 and 0.5m, respectively. By using six types of model, the effects of the widths and the elasticity of boards on deflections and motions of them can be examined.

Displacement of the center of each floating board must be measured in air to evaluate rigidity of each floating body. **Photograph 3** shows the situation of deformation measurement of a floating board at the center point of it. The rigidity of floating boards is estimated by use of the measured data. These values are also listed in **Table 1** as Young's moduli. For example, the rigidity of Model-A, B and C is 4.07, 4.10 and 4.03kN/cm^2, respectively. The rigidity of boards before coating on the surface of them is 3.16kN/cm^2. The coating makes the boards waterproof, and this causes the difference between measured rigidity and original one.

b) Method of model experiments

Figure 2 shows the experimental basin and equipment. The basin is 10m in width and about

19m in length. Two irregular wave generators are installed along one side, and wave-absorbing units are arranged along the other three sides. The model of a floating board is set at the center of the basin, and two wave gauges are installed to measure wave heights.

In the model experiments, the motions of a model are measured by use of a laser displacement meter and nine accelerometers. **Photograph 4** shows the arrangement of them around a floating body model in the basin. The laser displacement meter is fixed over the center of the floating board. The nine accelerometers are attached to the points of $+0.4L$, $+0.3L$, $+0.2L$, $+0.1L$, $0.0L$, $-0.1L$, $-0.2L$, $-0.3L$, and $-0.4L$ in the longitudinal direction of the board, respectively, where L is the length of the board. These are named AP-1 to AP-9 in sequence from the incoming direction of waves, respectively. AP-5 is, therefore, located just at the center of the floating body. Strains that are caused by motions of the floating board are also measured. Nine strain gauges named εP-1 to εP-9 are also installed at the same points of the board where the accelerometers are located.

The model scale employed in the model experiments is 1/100. **Tables 2** and **3** show the experimental conditions. Regular waves were adopted in the model experiments. The water depth in the experiments is 0.3m, and the incident wave periods vary from 0.8 to 2.6s at variants of 0.2s. The wave height in the experiments is 0.01m for all types of model. In Model-A, the experiments for the incident wave height of 0.02m were additionally conducted. In addition, the wave direction for all the models is 0degree that means the longitudinal direction of the board. In Model-B, the experiments for three wave directions, which are 0, 30, and 60degrees, were performed.

Photograph 5 shows the overview of the model of a floating body model and all sorts of measuring instruments arranged in the basin. The model shown here is Model-C. Meanwhile, **Photo 6** shows the situation of the model experiment in regular waves. The model is Model-A. It can be clearly seen that waves are coming toward the model from the right of the photograph.

(2) Results of Model Experiments

a) Time histories of accelerations and strains

Figure 3 shows time histories of measured vertical accelerations of Model-A. The wave height, period and direction are 0.01m, 1.0s and 0degree, respectively. The time histories of the accelerations obtained for the time of 100 to 106s are shown here. During this time, the motions of the floating body and incident regular waves keep a steady condition after initial unsteady transient waves decrease. It is easily understood from the figure that the amplitudes of vertical accelerations are different in relation to the points on the board and that there is the phase difference between randomly selected two time histories. High frequency components not corresponding to the incident wave frequency are also seen in the figure. This is considered to be due to the natural frequency components of the floating board. The maximum values of accelerations appear at both ends of the board (AP-1 and AP-9).

Figure 4 shows time histories of measured strains of Model-A. The wave conditions are the same as those in **Fig. 3**. It is found from this figure that the time histories of strains indicate the regular wave profiles and high frequency components cannot be observed. These properties differ from those of the accelerations. Moreover, the maximum strains appear near the center of the board (εP-6).

b) Effects of elasticity of floating body

Figure 5 shows the longitudinal distribution of maximum vertical accelerations of Model-A, B and C, and Model-D, E and F. The wave height, period and direction are 0.01m, 1.0s and 0degree, respectively. The horizontal axis denotes the ratio X/L of the position of the sensor X to the

length of the board L. Meanwhile, the vertical axis denotes the ratio $Amax(X)/H$ of the maximum vertical acceleration at each point ($Amax(X)$, Gal) to the wave height (H, cm). As seen in the figure, the maximum values of the accelerations for all the models have an inclination to appear near both ends of the floating boards (+0.4L and -0.4L). The reason for this is that the vertical motions of the floating bodies become large at these points because of the superposition of heave and pitch motions. From the comparison of Model-A and D that have the same dimensions and different elasticity, it is understood that the maximum vertical accelerations tend to become larger in the floating body with large elasticity.

Figure 6 shows the longitudinal distribution of maximum strains of Model-A, B and C, and Model-D, E and F. The wave conditions are the same as those in **Fig. 5**. The horizontal axis denotes the ratio X/L in the same way as **Fig. 5**. The vertical axis denotes the ratio $\varepsilon max(X)/H$ of the maximum strain at each point ($\varepsilon max(X)$) to the wave height (H, cm). It is obvious from the figure that the maximum values appear at the point of -0.1L for Model-A, B, E and F, and at the points of +0.2L and -0.2L for Model-C and D. From the comparison of Model-A and D that have the same dimensions and different elasticity, it is also recognized that the maximum strains tend to become larger in the floating body with large elasticity.

Figure 7 shows the maximum vertical accelerations at the center point (0.0L) of Model-A, B and C, and Model-D, E and F, for incident wave periods. The horizontal axis denotes the wave period, and the vertical axis denotes the ratio $Amax(0)/H$ of the maximum vertical acceleration at the center point ($Amax(0)$, Gal) to the wave height (H, cm). It is found from the figure that the maximum values of the accelerations appear for the different wave periods in each floating body. Model-C and F have the distinct maximum values of the accelerations near the wave periods of 1.6 and 1.4s, respectively. In these cases, it is supposed that the incident wave periods are close to the natural periods of floating boards. However, it should be noted that the maximum values of the accelerations have an inclination to become large, not at the center of the floating bodies, but at both ends of them.

Figure 8 shows the maximum strains at the center point (0.0L) of Model-A, B and C, and Model-D, E and F, for incident wave periods. The horizontal axis denotes the wave period, and the vertical axis denotes the ratio $\varepsilon max(0)/H$ of the maximum strain at the center point ($\varepsilon max(0)$) to the wave height (H, cm). From this figure, it is understood that the strains show the maximum values near the wave period of 1.2s, and that they become smaller when the wave period becomes longer. Furthermore, the maximum strains of Model-A, B and C with large elasticity are larger than those of Model-D, E and F with small elasticity.

Figure 9 shows the maximum displacements at the center point (0.0L) of Model-A, B and C, and Model-D, E and F, for incident wave periods. The displacements are measured by use of the laser displacement meter. The horizontal axis denotes the wave period, and the vertical axis denotes the ratio $Zmax(0)/H$ of the maximum vertical displacement ($Zmax(0)$, cm) to the wave height (H, cm). It is clearly recognized that the maximum displacements tend to increase when the wave period becomes longer. For instance, the displacements are larger than the wave height, for the wave periods of more than 1.6s in case of Model-A. Moreover, the maximum vertical displacements become smaller when the width of the floating board becomes wider for Model-A, B and C with large elasticity. On the other hand, the effects of the widths cannot be seen for Model-D, E and F with small elasticity.

3. SEPARATE SUPPORT TYPE ELASTIC FLOATING BODY

(1) Hydraulic Model Experiments

a) Models of floating body

A separate support type elastic floating body in hydraulic model experiments is made of a polyurethane board and a few aluminum cylindrical pontoons. The use of the polyurethane board aims at reproducing flexible properties of a superstructure in a floating bridge of this type.

The view of a floating body model employed here is illustrated in **Fig. 10**. This model is composed of one long rectangular board used as a superstructure and two or three cylindrical pontoons used as floating foundations. The length of the board is 1.8 or 2.8m. The pontoons are 0.3m in diameter, 0.3m in height, and 0.25m in draft. There are two mooring poles fixed at the bottom of the experimental basin as well. The mooring system is identical with that of the continuous pontoon type floating body. Namely, the floating body can freely move up and down in the vertical direction along the mooring poles in waves.

Table 4 shows five types of model. Length, width, height, mass, Young's modulus, the number of pontoons, span length between pontoons and the distinction of rigidity of each model are listed in this table. Although the floating body model must be essentially treated as an elastic body, both elastic and rigid floating body models were employed in the experiments to investigate the effects of elasticity of the superstructure on motions and deformations of models. The elastic superstructure is made of polyurethane having a unit weight of 200kg/m^3. Meanwhile, the rigid superstructure is made of an aluminum channel. Model-A and B are rigid floating bodies with two and three pontoons, respectively, while Model-C, D and E are elastic floating bodies with two, three and three pontoons, respectively.

b) Method of model experiments

Hydraulic model experiments were carried out in the same experimental basin as used for continuous pontoon type floating body models. In the experiments, two wave gauges were arranged in the same way.

Tables 5 and **6** show the experimental conditions. Regular waves were adopted in the experiments. The water depth in the model experiments is 0.5m, and the incident wave periods vary from 1.0 to 1.6s at variants of 0.2s. The wave height in the experiments is constant, and it is 0.03m. In addition, the wave directions for all the models are 0 and 30degrees. The wave direction of 0degree coincides with the longitudinal direction of the model. In Model-A, the experiments for the wave direction of 60degrees were additionally conducted. The model experiments were performed based on Froude similitude. Although the floating body models employed in the experiments are not manufactured for specific prototypes, the model scale is assumed to be 1/100.

Photograph 7 shows the arrangement of measuring instruments around a floating body model in the basin. The parameters measured in the model experiments are wave heights, and vertical accelerations, strains and displacements of the superstructure of the model. The vertical accelerations, strains and displacements are obtained by use of accelerometers, strain gauges and two laser displacement meters, respectively. These data are digitally recorded for the duration of 204.8s. For Model-A, B, C and D, seven accelerometers and strain gauges are attached to the points of $+0.35L$, $+0.21L$, $+0.07L$, $0.0L$, $-0.35L$, $-0.21L$, and $-0.07L$ in the longitudinal direction of the board, respectively. Herein, L is the length of the board. These are named AP-1 to AP-7 and εP-1 to εP-7 for accelerometers and strain gauges, respectively. On the other hand, for Model-E, eleven accelerometers and strain gauges are used. Besides, vertical displacements at two pontoon positions are observed by the laser displacement meters at the points of $+0.28L$ and $-0.28L$ for Model-A, B, C and D. These are named LP-1 and LP-2, respectively.

Photograph 8 shows the overview of a floating body model and all sorts of measuring instruments arranged in the basin. This shows the case of Model-E. Next, **Photo 9** shows the situation of deformation of the floating body model subjected to waves. Model-E is the model shown here.

(2) Results of Model Experiments

a) Time histories of accelerations and strains

Figure 11 shows time histories of measured vertical accelerations of Model-D. The wave height, period and direction are 0.03m, 1.6s and 0degree, respectively. The time histories of the accelerations are shown in this figure for the time of 100 to 106s. In the figure, the vertical accelerations at the points near the center of the board (AP-3 to AP-5) are larger than those at the points near both ends of it (AP-1, AP-2 and AP-6) except for the point of AP-7. It is also recognized that high frequency components, which are supposed to be the natural frequency components of the floating body, greatly affect the wave profiles of the accelerations. Therefore, the wave profiles of the accelerations disagree with the incident sinusoidal wave profile.

Figure 12 shows time histories of measured strains of Model-D. The wave conditions are the same as those in **Fig. 11**. It is clear from the figure that the time histories of strains are roughly regarded as sinusoidal wave profiles at the points between two side pontoons (εP-2 to εP-6). In addition, the strain amplitudes at these points are almost the same. The reason for this is that the deformations of the board following the incident regular waves are caused by three pontoons.

b) Effects of elasticity of floating body

Figure 13 shows the longitudinal distribution of maximum vertical accelerations of Model-B and D. The wave height, period and direction are 0.03m, 1.0s and 0degree, respectively. The horizontal axis denotes the ratio X/L of the position of the sensor X to the length of the board L. Meanwhile, the vertical axis denotes the ratio $Amax(X)/H$ of the maximum vertical acceleration at each point ($Amax(X)$, Gal) to the wave height (H, cm). The solid line represents the results of Model-B, while the dotted line represents the results of Model-D. Besides, three vertical solid lines in the figure mean the points where three pontoons are located. It can be obviously seen that the maximum values of the accelerations for these two models tend to appear at both ends of the boards. This is considered to be due to heave motions of three pontoons following the incident waves. Namely, in this case, the heave motions of the pontoons mainly cause the deformations of the boards. From the comparison of Model-B and D, it is also understood that the maximum vertical accelerations are relatively large in the floating body with large elasticity.

Figure 14 shows the longitudinal distribution of maximum strains of Model-B and D. The wave conditions are the same as those in **Fig. 13**. The horizontal axis denotes the ratio X/L, and the vertical axis denotes the ratio $\varepsilon max(X)/H$ of the maximum strain at each point ($\varepsilon max(X)$) to the wave height (H, cm). The lines shown in the figure represent the same ones as shown in **Fig. 13**. It is easily recognized that the maximum strains are large and almost constant at the points between two side pontoons for Model-D. On the other hand, the maximum strains of Model-B are very small as compared with those of Model-D, because of the large rigidity of the board. In other words, the maximum strains tend to become much larger in the floating board with large elasticity.

Figure 15 shows the maximum vertical accelerations at the center point ($0.0L$) of Model-B and D, for incident wave periods. The horizontal axis denotes the wave period, and the vertical axis denotes the ratio $Amax(0)/H$ of the maximum vertical acceleration at the center point ($Amax(0)$, Gal) to the wave height (H, cm). The solid line represents the results of Model-B,

while the dotted line represents the results of Model-D. From the figure, it is clear that the maximum values of the accelerations appear for the wave periods of 1.2 and 1.4s for Model-B and more than 1.2s for Model-D. It is also understood that the accelerations of Model-D with large elasticity are somewhat larger than those of Model-B with small elasticity for almost all the wave periods.

Figure 16 shows the maximum strains at the center point (0.0*L*) of Model-B and D, for incident wave periods. The horizontal axis denotes the wave period, and the vertical axis denotes the ratio $\varepsilon max(0)/H$ of the maximum strain at the center point ($\varepsilon max(0)$) to the wave height (*H*, cm). The lines shown in the figure represent the same ones as shown in **Fig. 15**. It can be seen from the figure that the maximum strains of Model-B are very small in comparison with those of Model-D in the same way as shown in **Fig. 14**. Moreover, the maximum strain of Model-D becomes larger when the wave period becomes longer. Consequently, the maximum strains of Model-D with large elasticity are larger than those of Model-B with small elasticity.

Figure 17 shows the maximum displacements at the point of LP-1 of Model-B and D, for incident wave periods. The horizontal axis denotes the wave period, and the vertical axis denotes the ratio $Zmax(+0.28L)/H$ of the maximum vertical displacement ($Zmax(+0.28L)$, cm) to the wave height (*H*, cm). The lines shown in the figure represent the same ones as shown in **Fig. 15**. It is recognized that the maximum vertical displacements are large for the wave periods of 1.2 and 1.4s for both models. Further, the displacements of both models show almost the same tendency for the wave periods. However, in case of Model-D, the displacements are slightly smaller than those of Model-B for the wave periods of more than 1.4s. Accordingly, the elasticity of the floating body models does not have much influence on the maximum displacements of them except for longer wave periods.

c) Effects of number of cylindrical pontoons

Figure 18 shows the longitudinal distribution of maximum vertical accelerations of Model-C and D. The wave height, period and direction are 0.03m, 1.0s and 0degree, respectively. The horizontal axis denotes the ratio *X*/*L*, and the vertical axis denotes the ratio $Amax(X)/H$. The solid line represents the results of Model-C with two pontoons, while the dotted line represents the results of Model-D with three pontoons. Besides, two vertical solid lines and three vertical dotted lines in the figure mean the points where two and three pontoons are located, respectively. It is found from the figure that in Model-C with two pontoons, the maximum vertical accelerations near the center of the board are considerably larger than those at both ends of it. Meanwhile, it is understood that in Model-D with three pontoons, the maximum vertical accelerations become larger at both ends of the board. In case of Model-C, since the vertical movements of two pontoons are generated by waves, the vertical deformation of the board becomes large near the center of it, and this causes the increase of the maximum vertical accelerations there. Meanwhile, Model-D has the short span lengths of 0.5m and one pontoon at the center point of the floating body. Namely, the vertical deformation of the board is restricted by the center pontoon, and this results in the decrease of the maximum vertical accelerations near the center of the floating body.

Figure 19 shows the longitudinal distribution of maximum strains of Model-C and D. The wave conditions are the same as those in **Fig. 18**. The horizontal axis denotes the ratio *X*/*L*, and the vertical axis denotes the ratio $\varepsilon max(X)/H$. The lines shown in the figure represent the same ones as shown in **Fig. 18**. It can be seen from the figure that the maximum strains have the flat distribution as a whole in case of Model-C with two pontoons. Furthermore, in case of Model-D with three pontoons, the maximum strains are

almost constant at the points between two side pontoons. From the comparison of Model-C and D, it is understood that the maximum strains are large in the floating body with three pontoons in this case.

4. CONCLUSIONS

The results of hydraulic model experiments on the continuous pontoon type and the separate support type elastic floating bodies were described in this paper. This is a fundamental study for realizing construction of long and large flexible floating structures such as floating bridges. The comparison of experimental and numerical results is a main subject to be performed after this.

Major knowledge obtained in the present study is summarized as follows:

(1) The continuous pontoon type floating body

a) In the time histories of vertical accelerations, high frequency components corresponding to the natural frequency components of the floating body are clearly observed. Conversely, the time histories of strains indicate the regular wave profiles.

b) The maximum vertical accelerations and strains tend to become larger in the floating body with large elasticity. The maximum displacements increase when the wave period becomes longer.

(2) The separate support type floating body

a) In the time histories of vertical accelerations, high frequency components corresponding to the natural frequency components of the floating body are recognized. On the other hand, the time histories of strains indicate the regular wave profiles at the points between two side pontoons.

b) The maximum vertical accelerations and strains tend to become larger in the floating body with large elasticity. The maximum displacements become larger for the middle wave periods.

c) The maximum vertical accelerations are remarkably large near the center point in the floating body with two pontoons. The maximum strains become larger in the floating body with three pontoons.

REFERENCES

Lwin,M.M.(1994): "Floating Bridges in the United States", *Proc. of International Workshop on Floating Structures in Coastal Zone, the Port and Harbour Research Institute*, pp.56-73.

Landet, E.(1994): "Planning and Construction of Floating Bridges in Norway", *Proc. of International Workshop on Floating Structures in Coastal Zone, the Port and Harbour Research Institute*, pp.43-45.

Shiraishi,S., Ishimi,G., Yoneyama,H. and M.Kondo(1996): "Experimental Study on Motions of Long Flexible Floating Structures in Waves", *Proc. of International Workshop on Very Large Floating Structures*, pp.265-273.

Shiraishi,S., Ishimi,G. and H.Yoneyama(1997a): "Experiment and Analysis on Motions of Long Flexible Floating Structures in Waves", *Proc. of 21st Joint Meeting UJNR, Marine Facility Panel*, pp.187-194.

Shiraishi,S., Ishimi,G., Yoneyama,H. and M.Kondo(1997b): "Experimental Study on Motions and Forces of Flexible Beam Floating Structures in Waves and Effect of Rigidity of Body", *Proc. of Civil Engineering in the Ocean*, Vol.13, pp.189-194, (in Japanese).

Maruyama,T., Kawamura,Y., Tsuda,T., Kishimoto,T., Tanaka,H. and Y.Yasuda(1998a): "Plan and Design of Yumeshima-Maishima Bridge –Movable Floating Bridge-", *Bridge and Foundation Engineering, Kensetutosyo*, Vol.32, No.2, (in Japanese).

Maruyama,T., Kawamura,Y., Tsuda,T., Takeda,S., Nakaji,E., Oka,S. and M.Tsuchiya(1998b): "Plan and Design of Yumeshima-Maishima Bridge –Movable Floating Bridge-", *Bridge and Foundation Engineering, Kensetutosyo*, Vol.32, No.3, (in Japanese).

Ishimi,G., Shiraishi,S. and H.A.Z.E. Din(1999): "Hydraulic Model Test on Elastic Floating Body Supported by Pontoons", *Technical Note of the Port and Harbour Research Institute*, No.930, (in Japanese).

Shiraishi,S., Ishimi,G. and H.A.Z.E.Din(1999): "Experimental Study on the Motion of Elastic Floating Body Supported by Pontoons", *Proc. of Advances in Structural Engineering and Mechanics*, (in press).

Table 1 Types of floating body model
(continuous pontoon type)

Model	Length (m)	Width (m)	Thickness (m)	Density (kg/m³)	E (kN/cm²)
A	2.0	0.1	0.02	98.0	4.07
B		0.2			4.10
C		0.5			4.03
D		0.1		200.0	16.27
E		0.2			15.59
F		0.5			15.53

Table 2 Experimental conditions (1)
(continuous pontoon type)

	Model	Prototype
Water Depth (m)	0.3	30.0
Wave Period (sec)	0.8, 1.0, 1.2, 1.4, 1.6, 1.8, 2.0, 2.2, 2.4, 2.6	8, 10, 12, 14, 16, 18, 20, 22, 24, 26
Wave Height (m)	0.01, 0.02	1.0, 2.0
Wave Direction (deg)	0, 30, 60	0, 30, 60

Table 3 Experimental conditions (2)
(continuous pontoon type)

Model	Wave Height (m)		Wave Direction (deg)		
	0.01	0.02	0	30	60
A	○	○	○		
B	○		○	○	○
C	○		○		
D	○		○		
E	○		○		
F	○		○		

Table 4 Types of floating body model
(separate support type)

Model	Body	Length (m)	Width (m)	Height (m)	Mass (kg)	E (kN/cm²)	Pontoon	Span Length (m)
A	Rigid	1.8	0.125	0.035 ([type)	5.23	-	2	1.0
B							3	0.5
C	Elastic		0.15	0.02	1.30	14.61	2	1.0
D							3	0.5
E		2.8			1.95	17.61		1.0

Table 5 Experimental conditions (1)
(separate support type)

	Model	Prototype
Water Depth (m)	0.5	50.0
Wave Period (sec)	1.0, 1.2, 1.4, 1.6	10, 12, 14, 16
Wave Height (m)	0.03	3.0
Wave Direction (deg)	0, 30, 60	0, 30, 60

Table 6 Experimental conditions (2)
(separate support type)

Model	Wave Direction (deg)		
	0	30	60
A	○	○	○
B	○	○	
C	○	○	
D	○	○	
E	○	○	

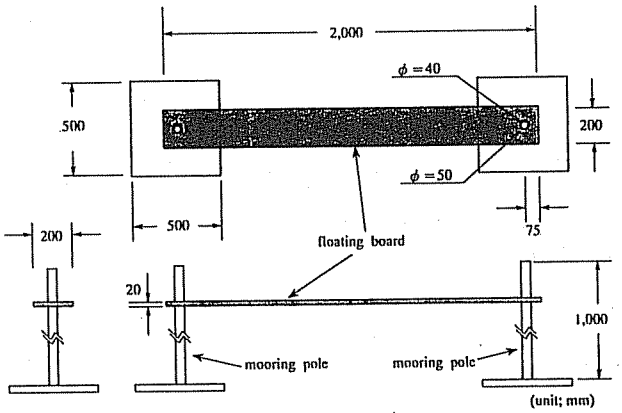

Fig.1 Experimental model
(continuous pontoon type; Model-B)

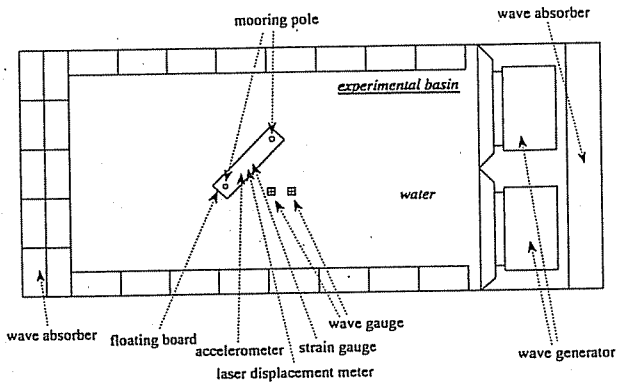

Fig.2 Experimental basin and equipment

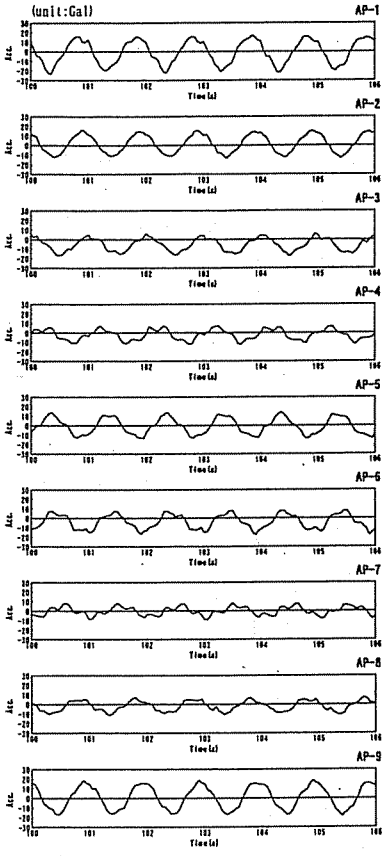

Fig.3 Time histories of vertical accelerations
(Model-A; H=0.01m, T=1.0s, θ=0deg)

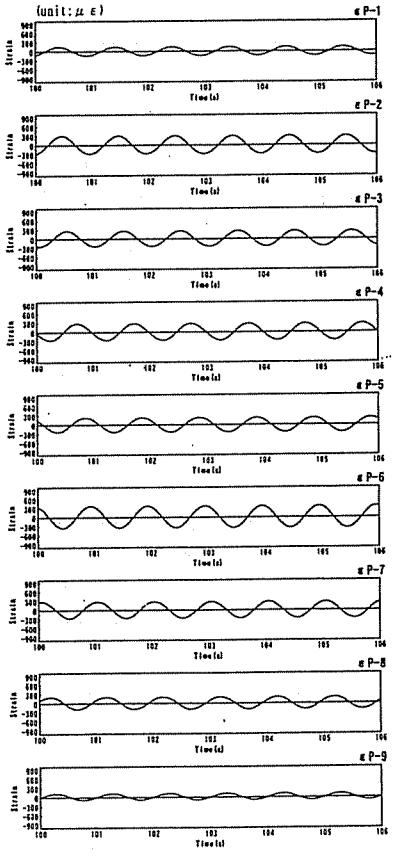

Fig.4 Time histories of strains
(Model-A; H=0.01m, T=1.0s, θ=0deg)

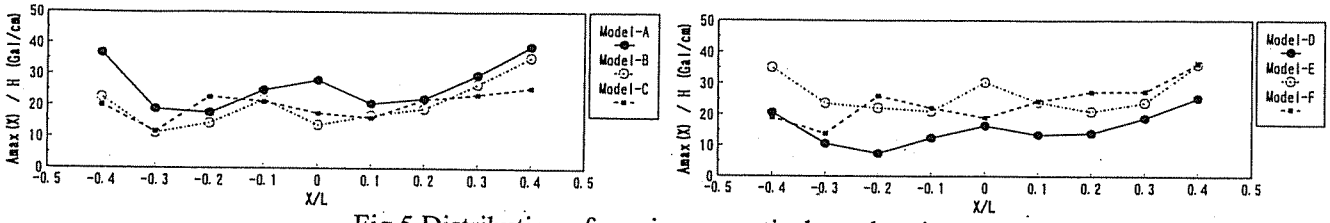

Fig.5 Distribution of maximum vertical accelerations
(Model-A, B, C and D, E, F; H=0.01m, T=1.0s, θ=0deg)

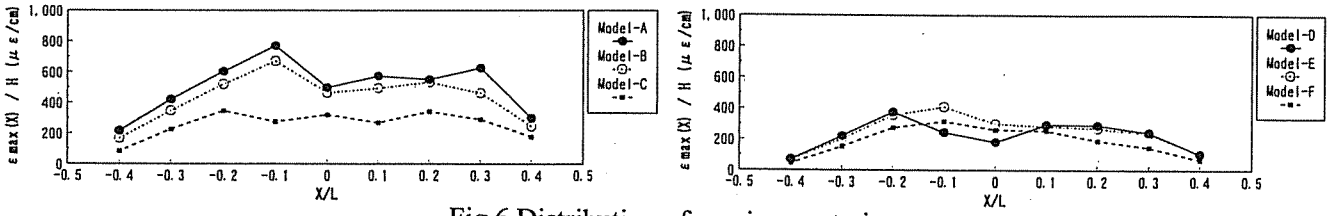

Fig.6 Distribution of maximum strains
(Model-A, B, C and D, E, F; H=0.01m, T=1.0s, θ=0deg)

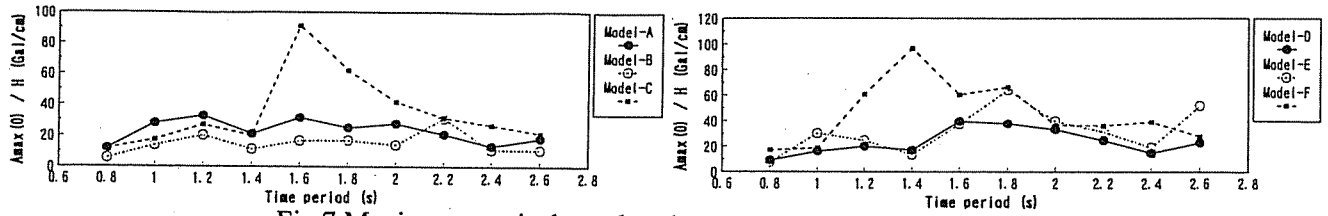

Fig.7 Maximum vertical accelerations at the center of floating body
(Model-A, B, C and D, E, F; H=0.01m, θ=0deg)

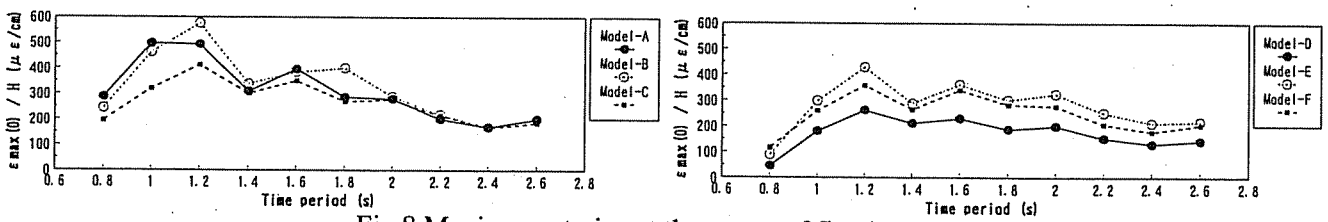

Fig.8 Maximum strains at the center of floating body
(Model-A, B, C and D, E, F; H=0.01m, θ=0deg)

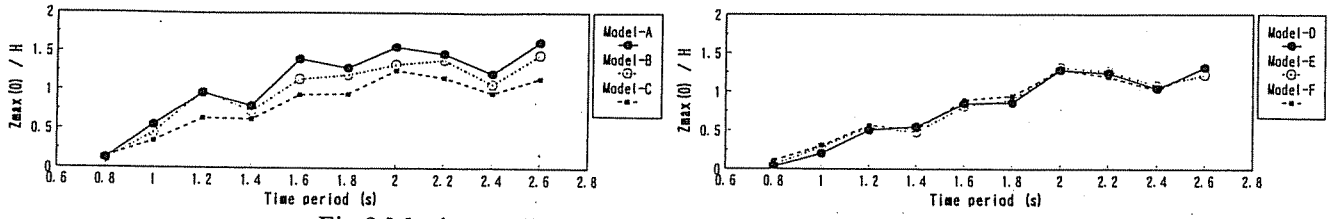

Fig.9 Maximum displacements at the center of floating body
(Model-A, B, C and D, E, F; H=0.01m, θ=0deg)

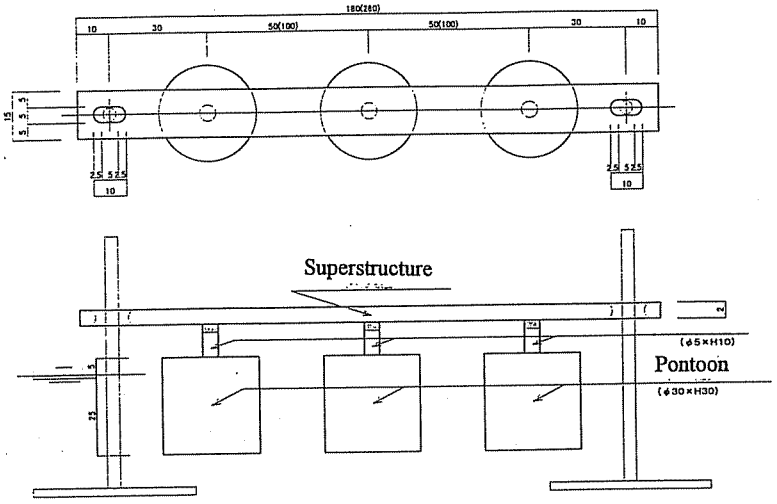

Fig.10 Experimental model
(separate support type)

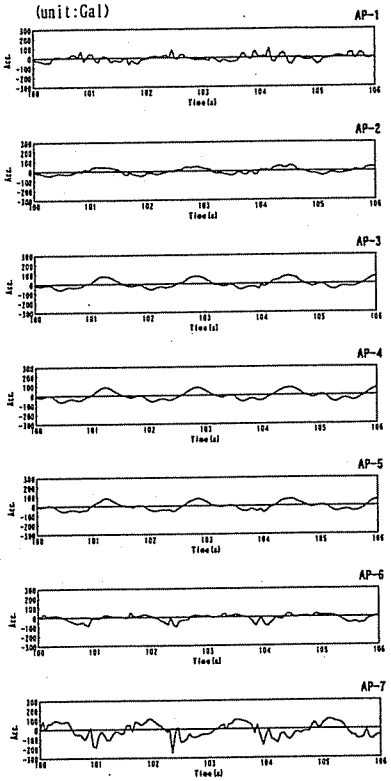

Fig.11 Time histories of vertical accelerations
(Model-D; H=0.03m, T=1.6s, θ=0deg)

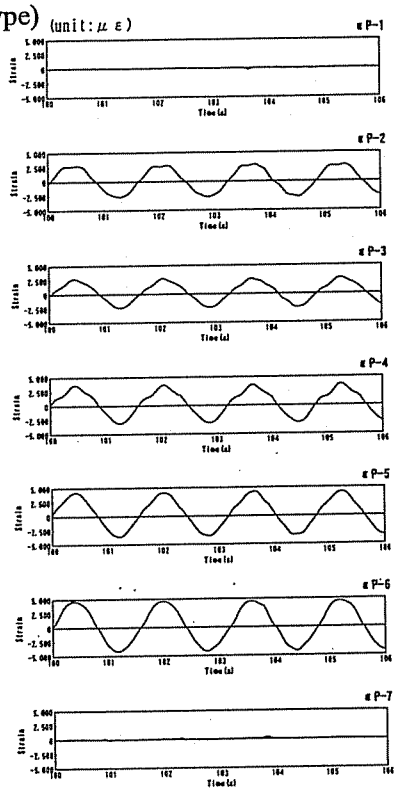

Fig.12 Time histories of strains
(Model-D; H=0.03m, T=1.6s, θ=0deg)

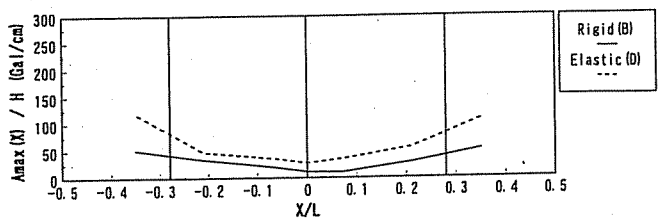

Fig.13 Distribution of maximum vertical accelerations
(Model-B and D; H=0.03m, T=1.0s, θ=0deg)

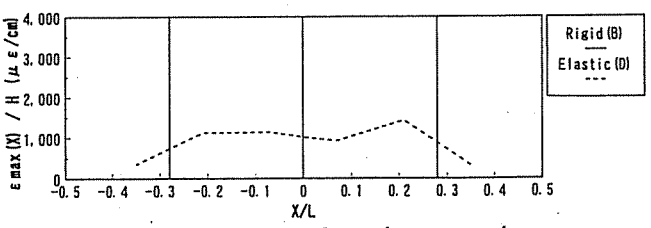

Fig.14 Distribution of maximum strains
(Model-B and D; H=0.03m, T=1.0s, θ=0deg)

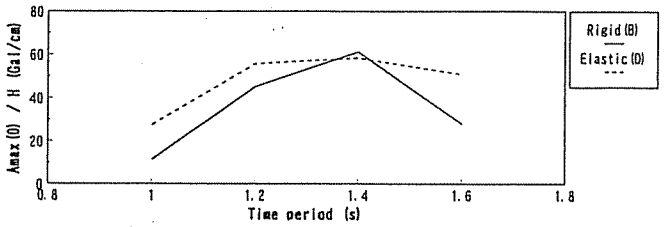

Fig.15 Maximum vertical accelerations at the center of floating body (Model-B and D; H=0.03m, θ=0deg)

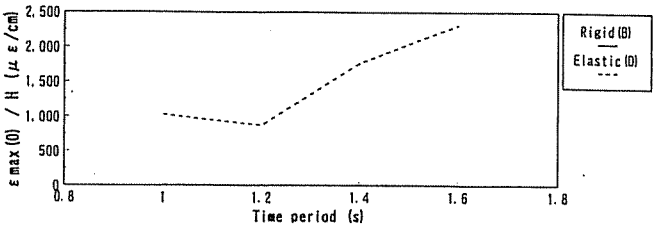

Fig.16 Maximum strains at the center of floating body (Model-B and D; H=0.03m, θ=0deg)

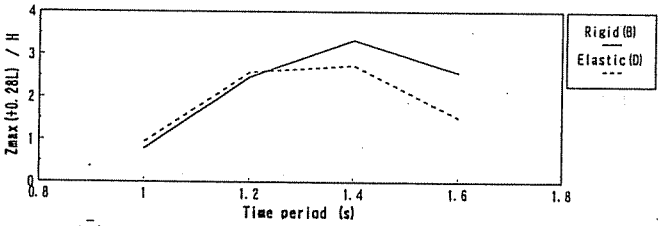

Fig.17 Maximum displacements at the point of LP-1 of floating body (Model-B and D; H=0.03m, θ=0deg)

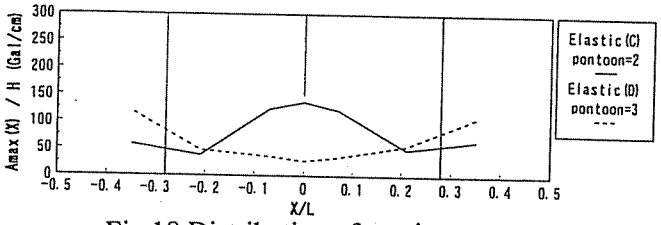

Fig.18 Distribution of maximum vertical accelerations (Model-C and D; H=0.03m, T=1.0s, θ=0deg)

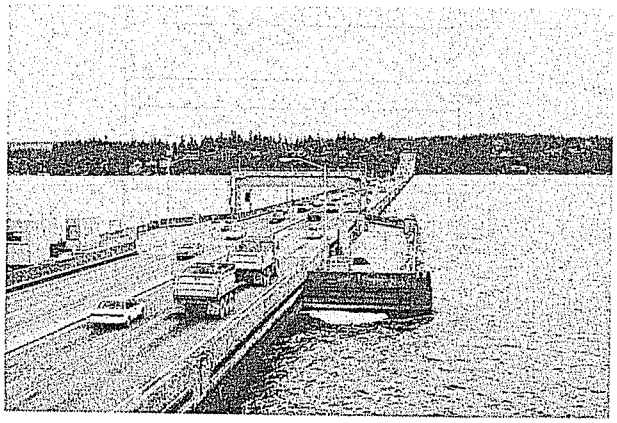

Photo 1 The Evergreen Point Bridge

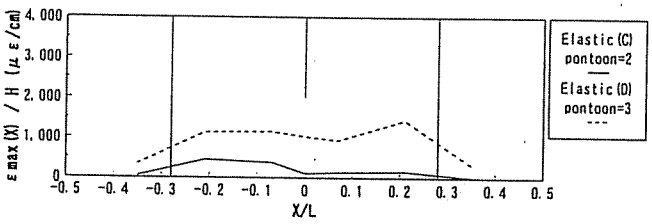

Fig.19 Distribution of maximum strains (Model-C and D; H=0.03m, T=1.0s, θ=0deg)

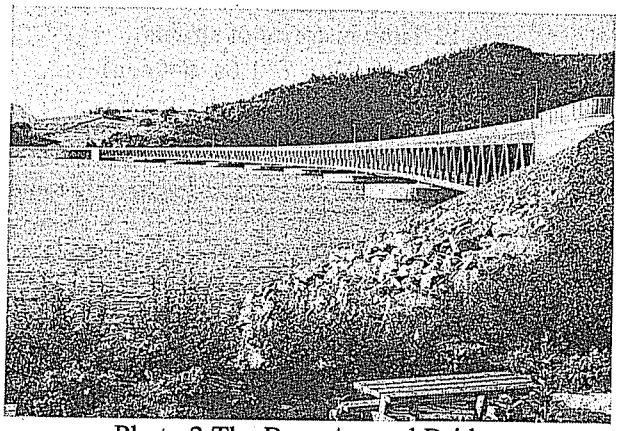

Photo 2 The Bergsφysund Bridge

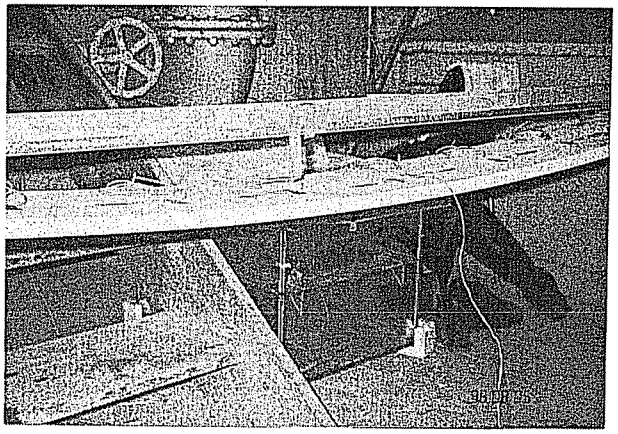

Photo 3 Deformation measurement of a floating board in air

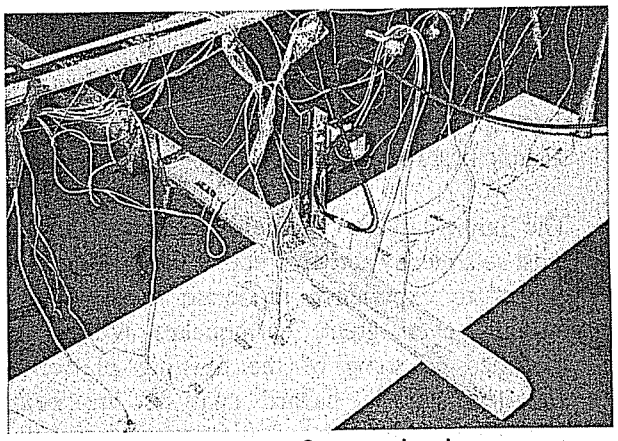

Photo 4 Arrangement of measuring instruments
(continuous pontoon type)

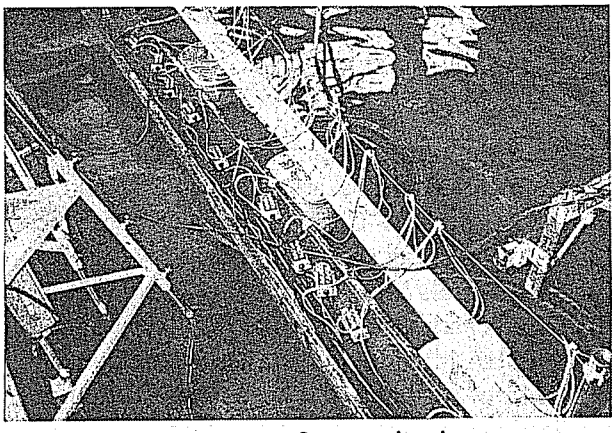

Photo 7 Arrangement of measuring instruments
(separate support type)

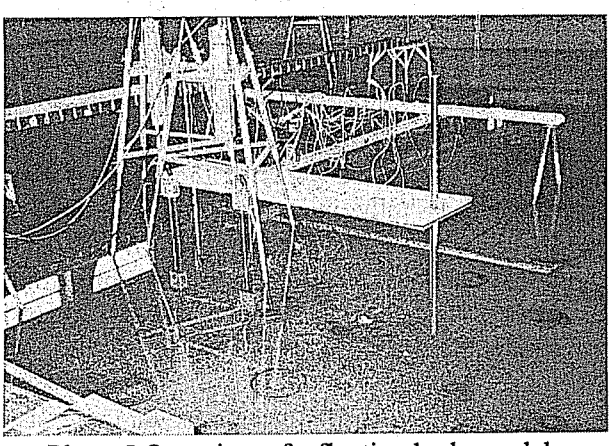

Photo 5 Overview of a floating body model
(continuous pontoon type)

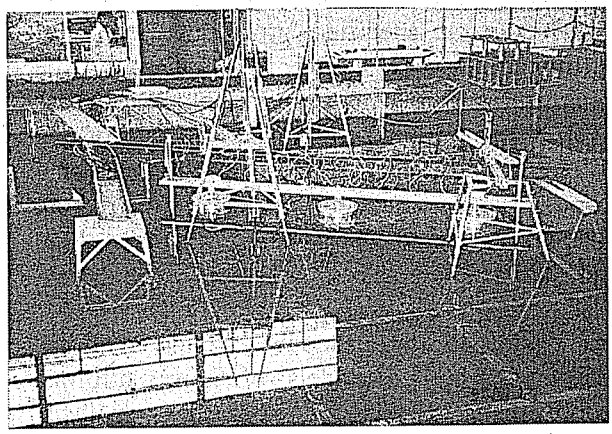

Photo 8 Overview of a floating body model
(separate support type)

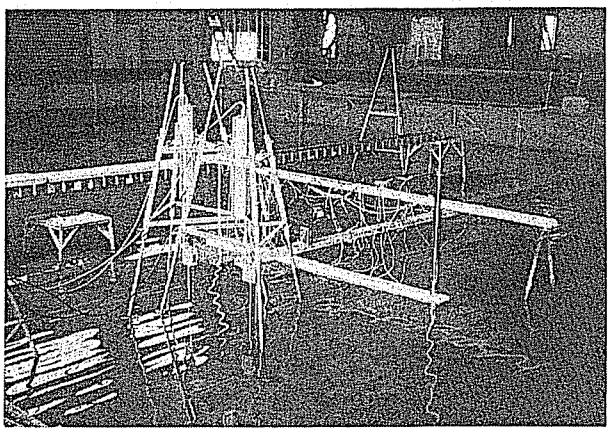

Photo 6 Situation of model experiments
(continuous pontoon type)

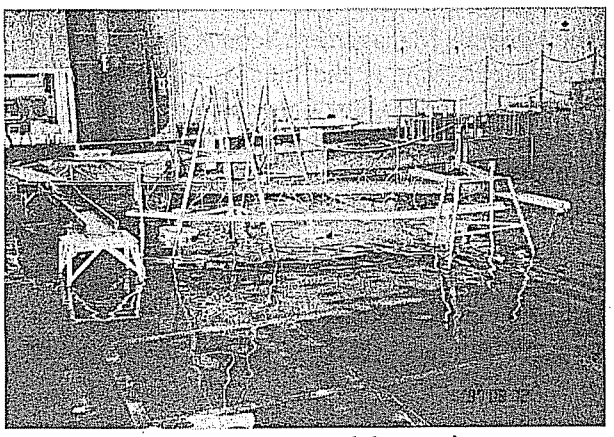

Photo 9 Situation of model experiments
(separate support type)